SUPPRESSION OF HIGH-AMPLITUDE NOISE VIA A T-X AMPLITUDE ATTENUATION METHOD

YIJUN YUAN[1], XUEMIN WU [2], CHUANZHANG TANG[3], YUE ZHENG[1] and YUN WANG[1]

[1] *School of Geophysics and Information Technology, China University of Geosciences, Beijing 100083, P.R. China. yyj@cugb.edu.cn*
[2] *Guangzhou Marine Geological Survey Bureau, Guangzhou 510075, P.R. China.*
[3] *Huabei Oilfield Company, Renqiu 062552, P.R. China.*

(Received September 10, 2018; revised version accepted September 8, 2019)

ABSTRACT

Yuan, Y., Wu, X.M., Tang, C.Z., Zheng, Y. and Wang, Y., 2019. Suppression of high-amplitude noise via a t-x amplitude attenuation method. *Journal of Seismic Exploration,* 28: 533-550.

High-amplitude noise in seismic data, especially tape-generated high-amplitude noise which was caused by tape magnetic powder loss during the storage of seismic data, contaminates the dataset and leads to large noise event in the prestack migration. To attenuate high-amplitude noise and reduce the effect of strong-energy noise on prestack migration, we have developed a method for the attenuation of high-amplitude noise in shot gathers. Based on the characteristics of high-amplitude noise, an amplitude attenuation equation (AAE) in the time-space (t-x) domain is used to suppress the energy of high-amplitude noise in seismic data. According to the proposed method, the average absolute amplitude within time window is calculated first. The average absolute amplitude obtained from the statistics is used as a threshold for judging high-amplitude noise. Then, we calculate the difference between the amplitude absolute value of each sample point and the threshold. Finally, the obtained difference is used as a variable of the amplitude attenuation function for suppressing high-amplitude noise. Tests on synthetic data and real data demonstrate the effectiveness of the proposed method for attenuation of high-amplitude noise.

KEY WORDS: seismic data, high-amplitude noise, attenuation, t-x domain.

0963-0651/19/$5.00

INTRODUCTION

Seismic data, especially in land data, are often contaminated with high-energy noise and spatially aliased due to noise bursts, cultural noise, air blasts, transmission errors, etc., which may obscure fine details and decrease the signal to noise (S/N) ratio of data (Ristau and Moon, 2001; Zhou and Garossino, 2005). Clean prestack gathers with enhanced the S/N ratio are an essential pre-requisite for prestack migration and AVO studies (Dutta, 2008). High-amplitude random noise can come from various sources (Liu et al., 2015). According to the period of the generating noise, we may classify random noise in seismic data into two categories. The first is called the source-generated noise, which is often unavoidable noise during seismic data acquisition. A poorly planted geophone, transient movements in the vicinity of the recording cable, and electrical noise could all cause some random noise (Yilmaz, 1987). The second category is tape-generated random noise, which is caused by tape magnetic powder loss during the long-time storage of raw data and stacked data. Tape-generated noise is often present in old seismic data. Compared with source-generated noise, tape-generated random noise has the characteristics of strong energy, short delay and wide distribution (Tyapkin and Ursin, 2005; Wang et al., 2006).

So far, many methods of random noise attenuation have been developed in either the t-x or a transformed domain and have been used for suppressing random noise (Liu et al., 2009c). These include the f-x prediction filter (Canales, 1984; Gulunay, 1986; Liu and Chen, 2013; Sacchi and Naghizadeh, 2009), t-x prediction filter (Abma and Claerbout, 1995; Fomel, 2002; Liu et al., 2015), Cadzow filtering (Trickett, 2003; Trickett and Burroughs, 2009; Yuan and Wang, 2011), Singular Spectrum Analysis (Oropeza and Sacchi, 2011; Chen and Sacchi, 2015), f-x projection filtering (Chen and Sacchi, 2017), and others. Currently, these methods are widely used in attenuation of random noise generated during data acquisition. However, they cannot do a good job of suppressing tape-generated high-amplitude noise.

The common high-amplitude noise attenuation methods can be summarized in the following three categories: (1) surgical mute (Yuan et al., 2005), (2) frequency-dependent amplitude attenuation (Cai, 1999; Yu et al., 2005; Stein and Langston, 2007; Niu, 2013), and (3) median filtering (Bednar, 1983; Anderson and McMechan, 1989; Duncan and Beresford, 1995; Liu et al., 2006). Under ideal conditions, these methods are robust in suppressing high-amplitude noise. Surgical mute is the simplest method among the methods above. It can completely remove the noise. However, it will lose effective signals during noise suppression. Therefore, surgical mute is only suitable to suppress data with small amounts of high-amplitude noise (Yuan et al., 2005). Cai (1999) proposed a frequency-dependent noise attenuation method. Noise is detected in different frequency ranges and then is suppressed only in the frequency band occupied by noise (Cai, 1999). When noise occurs in a local frequency range, this method is robust. However, in practice, since the tape-generated noise almost dominates the signals of data in whole frequency bands, this method does not work well.

Median filtering is a method widely used in suppressing high-amplitude noise (Bednar, 1983; Liu et al., 2006; Liu et al., 2008; Wang et al., 2012). The median filter runs through the signal entry by entry, replacing each entry with the median of neighboring entries. It can preserve edges while removing noise. However, while more than half the data are contaminated by high-amplitude noise, the median will not give an arbitrarily large or small result. Under this case, median filtering cannot completely suppress the high-amplitude noise. Wang et al. (2006) developed an adaptive attenuation method of seismic abnormal amplitude. In this method, a fractional function was defined as the attenuation coefficient of anomalous amplitude value to suppress noise. However, the fractional function is more sensitive to large anomalous amplitude values. If the sample point value is very big, the amplitude of sample points after attenuation is close to zero. Like the surgical mute method, this method easily damages reflection signals while suppressing high-amplitude noise (Wu et al., 2017).

Although high-amplitude attenuation has become a regular module in commercial seismic data processing software system for many years and some denoising methods are widely used in industry, the attenuation of tape-generated random noise is still a difficult problem. In this paper, we propose an approach based on the amplitude exponential attenuation function to suppress tape-generated high-amplitude noise in seismic data. Tests on synthetic data and real data show that this method is very robust for high-amplitude noise attenuation.

METHODS

Identification of high-amplitude noise

Identifying high-amplitude noise is the first step in the proposed method. First, we calculate the average absolute amplitude in a time window, which is selected according to the distribution of high-amplitude noise in shot records. The average absolute amplitude will be used as a threshold for judging high-amplitude noise. The equation for calculating the average absolute amplitude can be expressed as

$$M(k) = \frac{2}{nN} \sum_{i=1}^{n} \sum_{j=1}^{N} \left| A_0(i, j) \right|, \tag{1}$$

where n is the number of seismic traces in the time window, i denotes the *i-th* trace, N is the number of sampling points in the *i-th* trace, j is the *j-th* sampling point, $A_0(i, j)$ denotes the initial amplitude of the *j-th* sampling point in the *i-th* trace, and $M(k)$ denotes the threshold calculated in the *k-th* time window.

After obtaining the threshold, we can calculate the difference between the amplitude absolute value of each sample point in the time window and the threshold. The equation is written as follows

$$d(i,j) = \left|A_0(i,j)\right| - M(k), \tag{2}$$

where $d(i,j)$ denotes the difference between the absolute amplitude value of the *j-th* sample point in the *i-th* trace and the threshold $M(k)$. According to eq. (2), we judge whether the amplitude of sample point *j* is high-amplitude noise. If $d(i,j)$ is greater than zero, the amplitude of sample point *j* is considered high-amplitude noise; otherwise, it is considered a normal signal.

Definition of the amplitude attenuation equation

The stronger the energy of high-amplitude noise, the greater the degree of suppression of high amplitude noise. According to this rule, we define a t-x amplitude attenuation equation for suppressing the high-amplitude noise. The amplitude attenuation equation is written as follows

$$A(i,j) = A_0(i,j)e^{-d(i,j)}, \tag{3}$$

where $A(i, j)$ is the amplitude of the *j-th* sampling point in the *i-th* trace after noise is attenuated, $e^{-d(i,j)}$ is an exponential function of $d(i,j)$.

As seen in eq. (3), the degree of amplitude attenuation is positively correlated with the difference between the absolute value of sample point and the threshold; that is, the high-amplitude noise is attenuated exponentially with the increase of $d(i, j)$. The high-amplitude attenuation function can be defined as follows

$$c(i,j) = \begin{cases} e^{-d(i,j)} & d(i,j) > 0 \\ 1.0 & d(i,j) \le 0 \end{cases}, \tag{4}$$

where $d(i, j)$ denotes the difference obtained by eq. (2), and $c(i, j)$ denotes the amplitude exponential function for high-amplitude noise suppression.

Eq. (4) shows that if $d(i, j)$ is greater than zero, the amplitude of sampling point *j* is considered high-amplitude noise, and the function value is equal to $e^{-d(i,j)}$. If $d(i, j)$ is less than or equal to zero, the sampling point *j* is considered a normal signal, and the function value is equal to 1.0.

Attenuation of high-amplitude noise

In eq. (4), since the function value $c(i, j)$ is positively correlated with the value of noise, it can be used as an amplitude attenuation coefficient of noise to suppress high-amplitude noise. The equation of high-amplitude noise attenuation can also be written as follows

$$A(i,j) = A_0(i,j) \cdot c(i,j), \tag{5}$$

where $A_0(i, j)$ denotes the initial amplitude of the *j-th* sampling point in the *i-th* trace, $c(i, j)$ denotes the amplitude attenuation coefficient, and $A(i, j)$ denotes the amplitude after noise attenuation.

From eqs. (4) and (5), only those amplitudes larger than the threshold are attenuated. The degree of noise attenuation is related to the difference between the high-amplitude noise and the threshold. The larger the difference is, the higher the degree of attenuation. Sample points with amplitudes smaller than the threshold are not attenuated. Therefore, the threshold is a key parameter during noise attenuation. It must be greater than the amplitude absolute value of normal signals and less than the amplitude absolute value of noise. To ensure this, the time window must cover the areas including both normal signal and high-amplitude noise. In addition, in order to remove the effect of the noise above the first break on calculating the threshold, the noise above the first break will be muted before the statistical calculation.

Algorithm 1 shows the algorithm of identifying and suppressing high-amplitude noise in seismic data.

Inputs: A_0, N, i, j, n, k
Initializations: Z_A, A, M, d, c
  $Z_A(i,j)$=sort(abs(A_0(1:n, 1:N)))
  for i=1 to n **do**
    for j=1 to N/2 **do**
      $M(k)= M(k)+Z_A(i,j)$
    end for
  end for
  $M(k)=M(k)/((N/2)* n)$
  for i=1 to n **do**
    for j=1 to N **do**
      $d(i,j)$=abs($A_0(i,j)$)-$M(k)$
      if ($d(i,j)$>0) **then**
        $c(i,j)$=exp(-1*$d(i,j)$)
      else
        $c(i,j)$=1.0
      end if
      $A(i,j)= A_0(i,j)$ *c(i,j)
    end for
  end for
Output: $A(i,j)$

Algorithm 1. The algorithm of high-amplitude noise suppression

Fig. 1 shows a schematic flow chart of the high-amplitude noise attenuation. The main process includes the following steps

(1) Mute the noise above the first break of shot records.

(2) Determine the statistical time window. It must cover the area containing the normal amplitude and abnormal amplitude to ensure that the threshold is greater than the normal signal amplitude and less than the abnormal amplitude.

(3) Calculate the average absolute amplitude in the selected time window and use it as the threshold to judge whether it is high-amplitude noise.

(4) According to eq. (2), calculate the difference between the absolute value of each sample point and the threshold.

(5) Compute the amplitude attenuation coefficient by using the difference obtained in step (4).

(6) Attenuate high-amplitude noise by using the amplitude attenuation eq. (5).

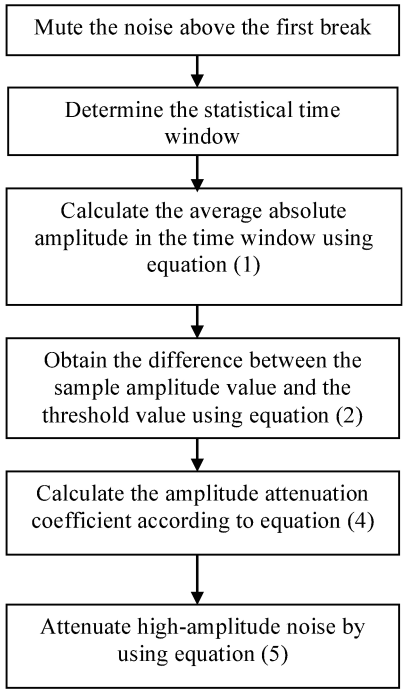

Fig. 1. Schematic flow chart for noise attenuation.

EXAMPLES

Synthetic data

Synthetic data are obtained on a four-layer horizontal layered medium model by using forward modeling of the acoustic wave equation. To verify the validity and applicability of the proposed method, different types of high-amplitude noise are added in synthetic data. Fig. 2a shows a synthetic shot record. Larger-amplitude noise is added from trace 40 to trace 50 in the shot gather. Note that the reflection signals are completely submerged by this strong-energy noise. According to the processing flow shown in Fig. 1, we use t-x AAE to suppress the noise of the shot gather. Fig. 2b is the result after noise attenuation. Notice that the strong-energy noise has completely disappeared and that the reflection signals covered by noise are better recovered. Fig. 2c shows the noise removed from Fig. 2a. As seen in Fig. 2c, reflection events originally in Fig. 2a are invisible. Fig. 2d is the result after using the fractional function attenuation method. In Fig. 2d, we see that the energy of the reflection signals between trace 40 and trace 50 is close to zero. In comparison to t-x AAE, this method damages more signals.

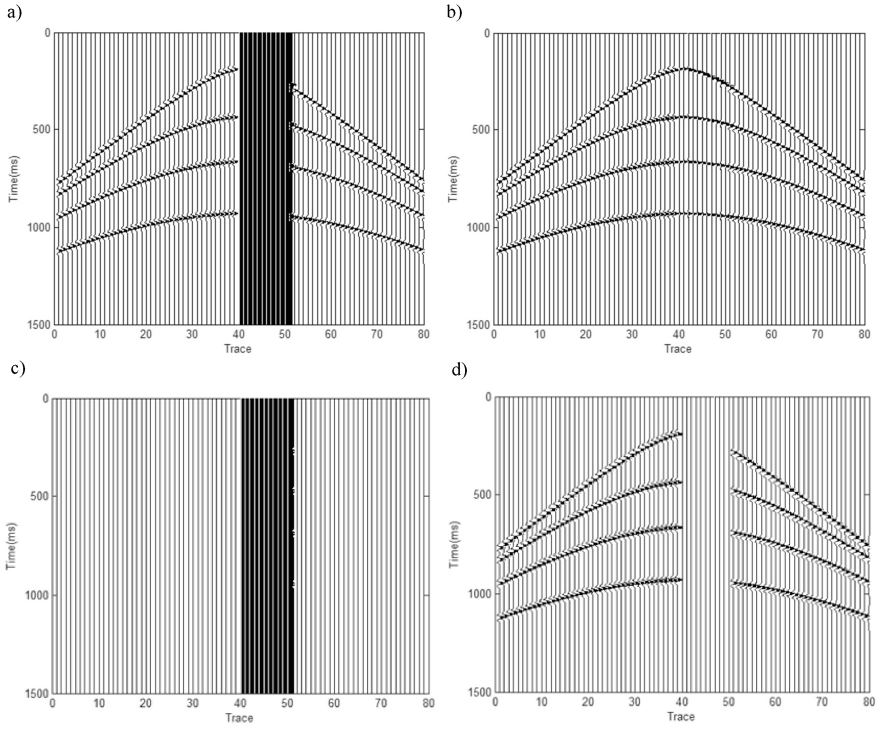

Fig. 2. Comparison of two noise-attenuation methods. (a) Synthetic shot record with high amplitude noise, (b) the result after applying t-x AAE, (c) the difference between the raw synthetic shot record and the result corresponding to (b), and (d) the result after using the fractional function.

Fig. 3a shows another synthetic shot record. A small amount of isolated noise is added to this shot record. Note that the isolated noise randomly distributes in the shot record. Compared to the amplitude of neighboring traces, the isolated noise has the characteristics of strong energy. Fig. 3b shows the result after using t-x AAE to suppress the isolated noise. Note that the energy of the isolated noise is greatly attenuated. Fig. 3c shows the removed noise. It is evident from Fig. 3c that there are no reflection signals present. Synthetic data examples show that the proposed method can be used for high-amplitude noise attenuation in shot records.

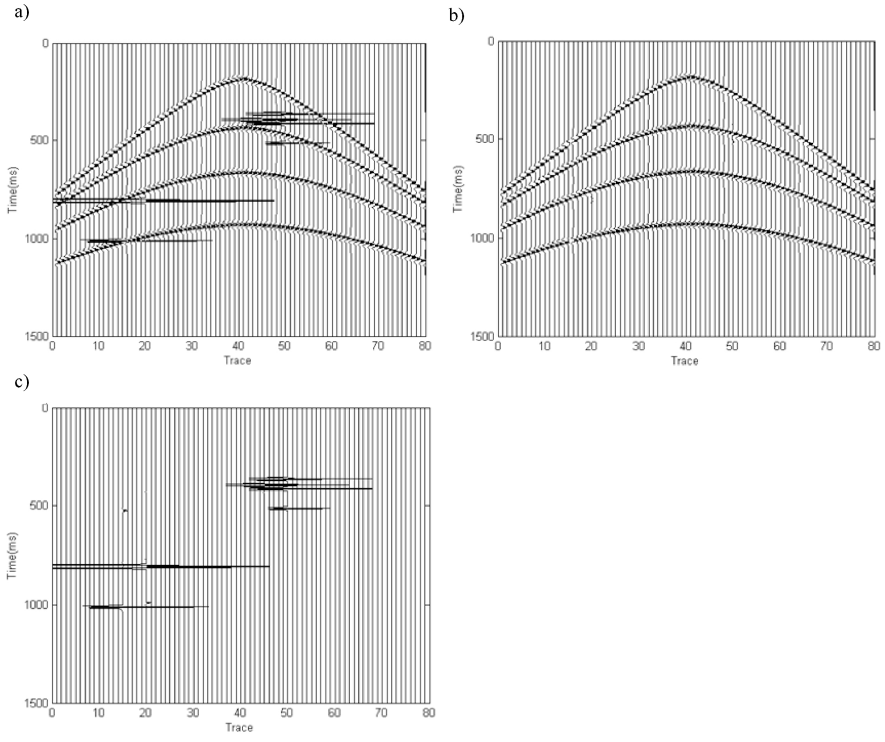

Fig. 3. Attenuation of isolated random noise. (a) A synthetic shot record containing some isolated high-amplitude noise, (b) the result after applying t-x AAE, and (c) the difference between (a) and (b).

Real data

In this section, we demonstrate the performance of the proposed method in suppressing both the source-generated noise and the tape-generated noise in real data, and we also compare t-x AAE with common-used commercial seismic data processing software.

Fig. 4a shows a shot record from a land 2D line acquired in 1996. The input data were 6 s long with 120 traces, and only the first 4.0 s of the shot record are displayed. To maintain the energy of the noise and signal in the raw data, the shot records do not apply AGC. It is evident from Fig. 4a that the amplitudes of trace 64 and trace 65 are much stronger than those of neighboring traces. According to their seismic characteristics, they belong to source-generated abnormal amplitude.

Fig. 4b shows the result after applying t-x AAE to the shot record shown in Fig. 4a. Note that the energy of trace 64 and trace 65 in the shot record is greatly attenuated, and the amplitude after noise attenuation is basically consistent with that of the neighboring traces. Fig. 4c shows the noise removed. Note that no reflection signals are present in Fig. 4c. This example shows that t-x AAE can attenuate the source-generated high-amplitude noise.

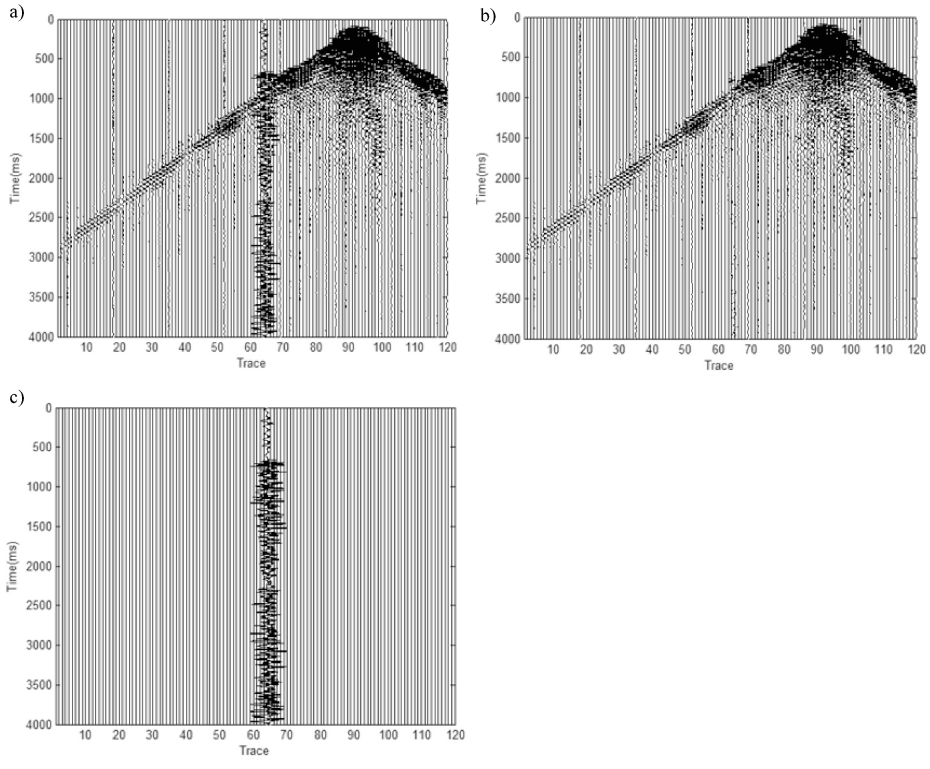

Fig. 4. Attenuation of source-generated abnormal amplitudes. (a) The shot record containing abnormal amplitudes, (b) the denoised result corresponding to (a), and (c) the removed noise.

Fig. 5a shows a shot record from another land 2D line, which was acquired in 2000. The input shot gather was 6 s long with 120 traces. Due to the effect of temperature and humidity on the magnetic tape storing seismic data, magnetic powder fell off while reading data from the tape. Notice that high-amplitude noise caused by the loss of tape magnetic powder dominates signals of the shot record. To reduce the effect of noise above the first break on the threshold calculation, the shot record is muted along the first break. Fig. 5b shows the result after muting. Fig. 5c shows the result after applying t-x AAE. Note that high-amplitude noise disappeared completely in Fig. 5c. Fig. 5d shows the difference between Figs. 5b and 5c. Notice that no reflection signals are visible in Fig. 5d.

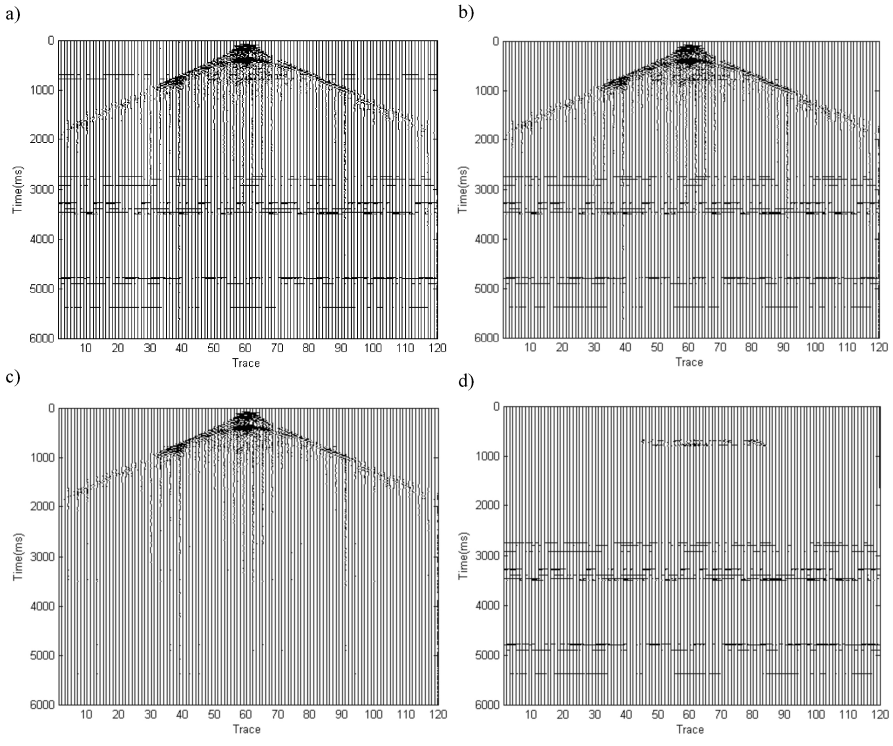

Fig. 5. Attenuation of tape-generated noise in real data. (a) The raw shot record, (b) the muted result corresponding to (a), (c) the denoised result processed with t-x AAE, and (d) the removed noise corresponding to (b).

Fig. 6a shows a shot record from a land 2D line, which was acquired in 1989. There are 120 traces in the shot record. The input data are 6 s long, and only the first 4.0 s of the shot record is displayed. Note that a large amount of high-amplitude noise caused by tape magnetic powder loss completely overwhelmed effective signals of the shot gather below 1.2 s. Fig. 6b shows the muted result. Fig. 6c shows the result after applying t-x

AAE. Note that the energy of high-amplitude noise in the shot record below 1.2 s is significantly reduced. We also find that the amplitude characteristic after noise attenuation is basically consistent with the amplitude attenuation characteristics of seismic wave propagation underground. In other words, the amplitude energy decreases with the increase in the seismic wave propagation distance. Fig. 6d shows the removed high-amplitude noise. Note that the removed noise is only present below 1.2 s, and there is no noise or signal beyond 1.2 s. This example further shows that the proposed method basically does not damage the reflection signals.

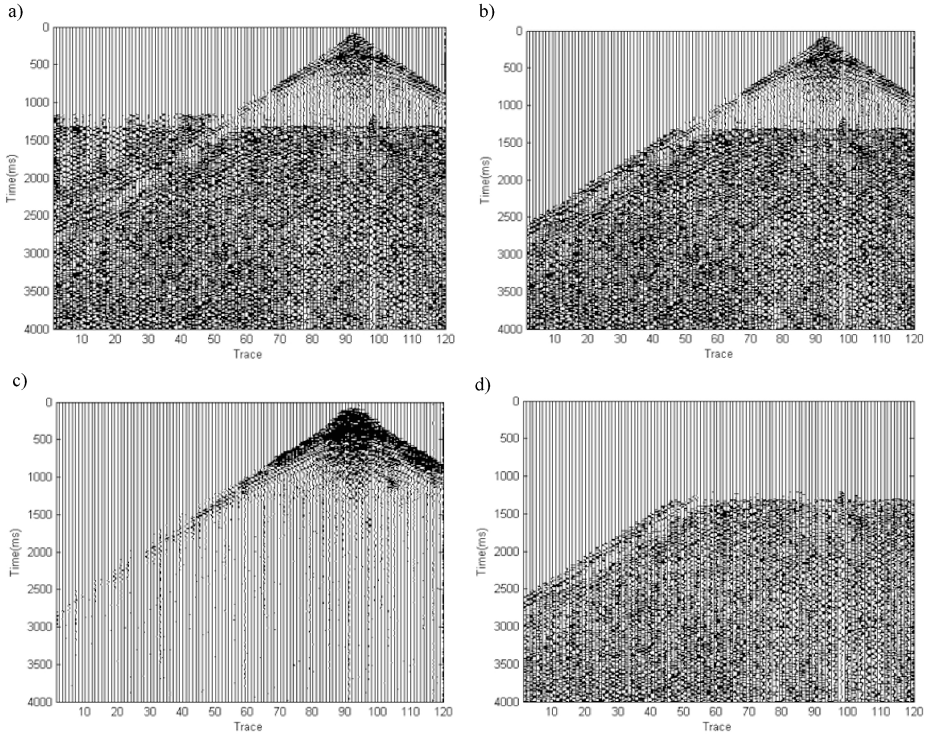

Fig. 6. Attenuation of tape-generated noise. (a) The shot record with high-amplitude noise, (b) the muted shot record, (c) the result after t-x AAE, and (d) the removed noise corresponding to (b).

The following examples illustrate how t-x AAE compares with two common-used methods. Fig. 7a shows the result after applying the frequency-dependent amplitude suppression method to the shot record shown in Fig. 6b. Note that a large amount of residual noise exists in the shot record below 1.2 s. Because tape-generated high-amplitude noise is randomly distributed in almost all frequency bands, the frequency-dependent amplitude suppression method cannot do a good job. Fig. 7b shows the result after applying median filtering to the same shot record shown in Fig. 6b. As seen in Fig. 7b, median filtering may suppress more noise than the

frequency-dependent amplitude suppression method. However, because more than half of the data are contaminated, a lot of residual high-amplitude noise still exists in the shot record. Compared to these two common-used methods, the t-x AAE method can obtain better results for tape-generated noise attenuation.

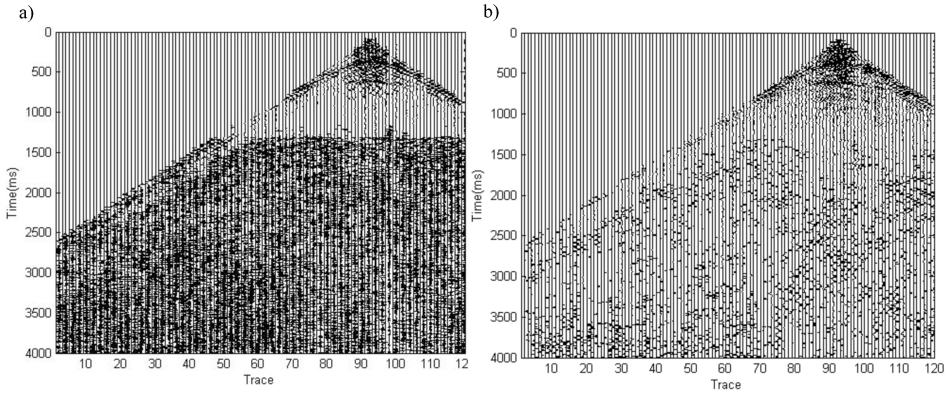

Fig. 7. The results processed by two common-used methods. (a) The shot record after frequency-dependent amplitude attenuation and (b) the shot record after median filtering.

Fig. 8 compares the waveforms of the 90-th trace extracted from the data of the original, AAE, frequency-dependent amplitude attenuation and median filtering, respectively. Signal with noise corresponding to Fig. 6b, denoising in t-x to Fig. 6c, denoising in f-x to Fig. 7a, and median filtering to Fig. 7b. Note that the energy of high-amplitude noise is obviously suppressed by AAE and the waveforms before 1.2 ms are more consistent with that of original data. For the frequency-dependent amplitude attenuation and median filtering denoising methods, they modified the waveforms of data before 1.2 ms at different degrees and the energy of residual high-amplitude noise after 1.2 ms are still strong.

To quantitatively evaluate the effectiveness of denoising, we use the S/N ratio to compare the results before and after noise attenuation. The Appendix gives a detailed instruction about the calculation of the S/N ratio spectrum. Fig. 9 shows the S/N ratio spectra of the shot records shown in Fig. 6b and Fig. 6c. The S/N ratio spectra are calculated in the same time window. The red curve corresponds to the S/N ratio of the shot record shown in Fig. 6b, and the blue curve corresponds to the S/N ratio of the shot record shown in Fig. 6c. As seen in Fig. 9, the smallest S/N ratio of the input data without noise attenuation is near 0 dB and the biggest is approximately 0.9 dB in [10,40] Hz, which includes effective signals. After noise attenuation by t-x AAE, the smallest S/N ratio is approximately 0.2 dB and the biggest is approximately 2.25 dB in [10,40] Hz. From Fig. 9, the S/N ratio after noise attenuation is obviously higher than the S/N ratio before noise attenuation in [10,40] Hz. Therefore, the proposed method can improve the S/N ratio of the data.

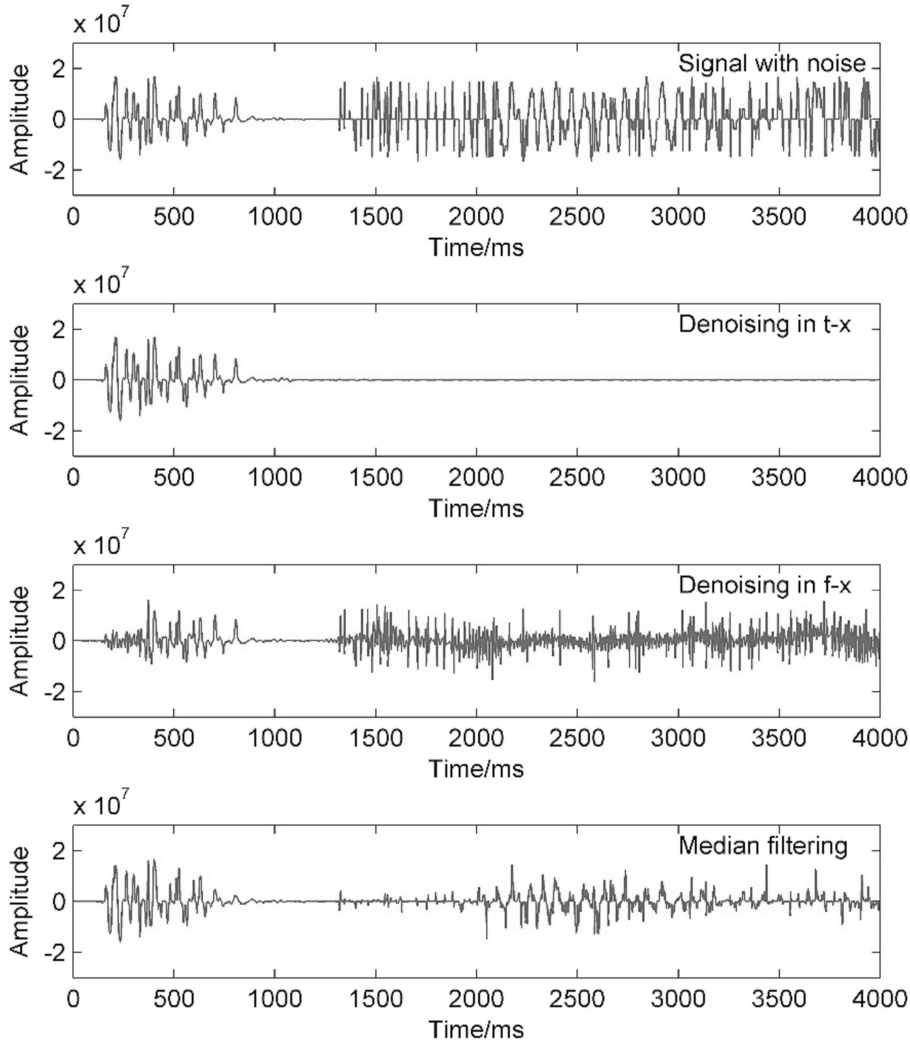

Fig. 8. Comparison of the waveforms of a single trace extracted from the data shown in Fig. 6 and Fig. 7. Signal with noise corresponding to Fig. 6b, denoising in t-x to Fig. 6c, denoising in f-x to Fig. 7a, and median filtering to Fig. 7b.

In the next examples, we demonstrate the application of the proposed noise suppression techniques to the prestack migration of the shot gathers from the land 2D line above. In data processing, a standard processing sequence was applied to the data: geometry analysis, ground roll denoising, preliminary spherical divergence correction, deconvolution, standard velocity analysis, and NMO correction and migration. The processing sequences and parameters are completely identical except for the process of high-amplitude noise attenuation.

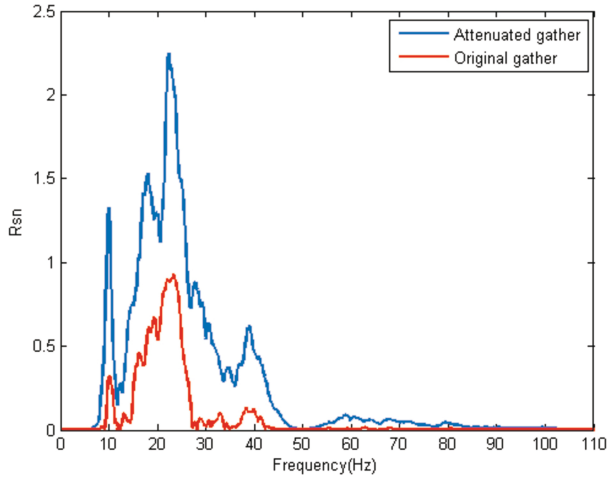

Fig. 9. S/N ratio spectra before and after noise attenuation. The red line corresponds to the data shown in Fig. 6b, and the blue line corresponds to the data shown in Fig. 6c.

Fig. 10a shows a prestack time migration section processed with no application of high-amplitude noise attenuation to prestack data. The input shot gathers used in prestack migration are shown in the shot record of Fig.5b. Note that some large noise events caused by high-amplitude noise during migration are present in Fig. 10a and cross with the neighboring reflection events. Fig. 10b shows the migration section after high-amplitude noise attenuation in the shot gathers. Notice that all of the large noise events completely disappeared and that the continuity of reflection events is greatly improved after high-amplitude noise attenuation.

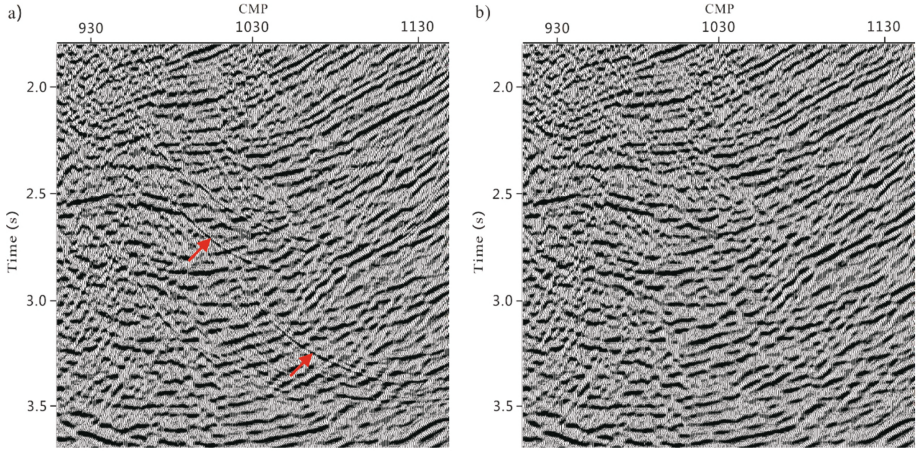

Fig. 10. Prestack time migration sections. (a) The migration section corresponding to the shot record shown in Fig. 5b and (b) the migration section corresponding to the shot record shown in Fig. 5c.

Fig. 11a shows another prestack time migration section with no application of high-amplitude noise attenuation to prestack gathers. The input shot gathers used in prestack migration are shown in the shot record of Fig. 6b. Compared to Fig. 10a, more large noise events appear in Fig. 11a due to the effect of strong-energy noise on migration. Fig. 11b shows the migrated section after applying t-x AAE to the prestack gathers. In comparison to Fig. 11a, there is significant attenuation of the noise in the migration section and good recovery of the reflections around the position of removed noise in Fig. 11b. These real examples show that attenuation of high-amplitude noise in the prestack gathers can reduce the effect of high-amplitude noise on migration.

CONCLUSIONS

We introduce a method to AAE for high-amplitude noise attenuation in the t-x domain. The method uses an adaptive amplitude attenuation equation to suppress strong-energy random noise in shot gathers. In the application of t-x AAE to suppress high-amplitude noise, the threshold is a key parameter. It directly affects the degree of noise attenuation. Synthetic data and real data examples show that the proposed method enhances the signal-to-noise ratio of shot gathers. Attenuation of high-amplitude noise in the prestack data reveals an improvement in the migration section. The application of this technique cannot only handle source-generated high-amplitude noise, but also suppress tape-generated strong-energy random noise. Compared to other conventional methods of high-amplitude noise attenuation, the proposed method is more effective in the attenuation of tape-generated strong-energy noise.

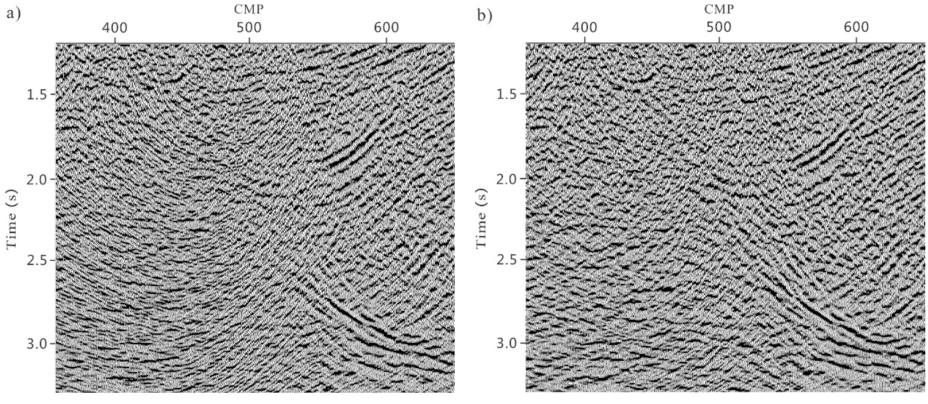

Fig. 11. Prestack time migration sections. (a) The migration section corresponding to the shot record shown in Fig. 6b and (b) the migration section corresponding to the shot record shown in Fig. 6c.

ACKNOWLEDGMENTS

We would like to thank Yingcai Li and Jianjun Gao for helpful discussions. The authors are particularly grateful to the reviewer for his review of this paper. This work is financially supported by National Natural Science Foundation of China (41974157, 41425017) and Hubei Oil Field Co.

REFERENCES

Abma, R. and Claerbout, J., 1995. Lateral prediction for noise attenuation by t-x and f-x technique. Geophysics, 60: 1187-1896.

Anderson, R.G. and McMechan, G.A., 1989. Automatic editing of noisy seismic data. Geophys. Prosp., 37: 875-892.

Bednar, J.B., 1983. Applications of median filtering to deconvolution, pulse estimation, and statistical editing of seismic data. Geophysics, 48: 158-161.

Cai, X., 1999. An effective method to suppress acoustic wave and high energy noise frequency-divisionally and adaptively. Oil Geophys. Prosp., 34: 373-380.

Canales, L., 1984. Random noise reduction. Expanded Abstr., 54th Ann. Internat. SEG Mtg., Atlanta: 525-527.

Chen, K., and Sacchi, M.D., 2015. Robust reduced-rank filtering for erratic seismic noise attenuation. Geophysics, 80(1): V1–V11.

Chen, K. and Sacchi, M.D., 2017. Robust f-x projection filtering for simultaneous random and erratic seismic noise attenuation: Robust f-x projection filter. Geophys. Prosp., 65: 650-668.

Claerbout, J., 1992. Earth Soundings Analysis: Processing versus Inversion. Blackwell Scientific Publications, Oxford.

Duncan, G. and Beresford, G., 1995. Median filter behavior with seismic data. Geophys. Prosp., 43: 329-345.

Dutta, S., 2008. Attenuation of high amplitude noise in prestack data and preservation of relative amplitude - a case study. 7th Internat. Conf. Exposit. Petrol. Geophys.: 90.

Fomel, S., 2002. Applications of plane-wave destruction filters. Geophysics, 67: 1946-1960.

Fomel, S. and Liu, Y., 2010. Seislet transform and seislet frame. Geophysics, 75(3): V25-V38.

Gulunay, N., 1986. FXDECON and complex Wiener prediction filter. Expanded Abstr., 56th Ann. Internat. SEG Mtg., Houston: 279-281.

Liu, C., Liu, Y., Yang, B., Wang, D. and Sun, J., 2006. A 2D multistage median filter to reduce random seismic noise. Geophysics, 71: V105-V110.

Liu, G.C. and Chen, X.H., 2013. Noncausal f-x-y regularized nonstationary prediction filtering for random noise attenuation on 3D seismic data. J. Appl. Geophys., 93: 60-66.

Liu, Y., Liu, C., Wang, D., Li, Q.X. and Feng, X., 2008. Application of time-variant median filtering technique to attenuation of seismic random noises. Oil Geophys. Prosp., 43: 327-332.

Liu, Y., Liu, N. and Liu, C., 2015. Adaptive prediction filtering in t-x-y domain for random noise attenuation. Geophysics, 80(1): V13-V21.

Liu, Z., Chen, X. and Li, J., 2009c. Noncausal spatial prediction filtering based on an ARMA Model. Appl. Geophys., 62: 122-128.

Oropeza, V.E. and Sacchi, M.D., 2011. Simultaneous seismic data denoising and via reconstruction multichannel singular spectrum analysis (MSSA). Geophysics, 76(3): V25-V32.

Niu, H., 2013. Application of frequency-dependent amplitude attenuation method to suppress strong-energy noise in offshore seismic data. Geophys. Prosp. Petrol., 52: 394-401.

Ricker, N., 1953. The form and laws of propagation of seismic wavelets. Geophysics, 18: 10-40.368.
Ristau, J.P. and Moon, W.M., 2001. Adaptive filtering of random noise in 2-D geophysical data. Geophysics, 66: 342-349,
Sacchi, M.D. and Naghizadeh, M., 2009. Adaptive linear prediction filtering for random noise attenuation. Expanded Abstr., 79th Ann. Internat. SEG Mtg., Houston: 3347-3351.
Stein, J.A. and Langston, T., 2007. Workshop: A review of some powerful noise elimination techniques for land processing. 69th EAGE Conf., London.
Trickett, S., 2003. F-xy eigenimage noise suppression. Geophysics, 68: 751-759.
Trickett, S. and Burroughs, L., 2009. Prestack rank-reducing noise suppression: theory. Expanded Abstr., 79th Ann. Internat. SEG Mtg., Houston: 3332-3336.
Tyapkin, Y. and Ursin, B., 2005. Optimum stacking of seismic records with irregular noise. J. Geophys. Engineer., 2: 177-187.
Wang, S.Q., Meng, X.H., Wang, J M., Cui, F.L., He, Y.S. and Chen, X.J., 2006. Seismic abnormal amplitude self-adapting inhibition. Petrol. Geol. Oilf. Devel. Daqing, 25: 112-116.
Wang, W., Gao, J.H., Chen, W.C. and Zhu, Z.Y., 2012. Random seismic noise suppression via structure-adaptive median filter. Chin. J. Geophys (in Chinese), 55: 1732-1741.
Wu, X.M., Yuan, Y.J. and Li, H., 2017. Anomalous amplitudes attenuation based on the seismic wave propagation theory. CGS/SEG Internat. Geophys. Conf., Qingdao, China.
Yilmaz, Ö., 1987. Seismic Data Processing. SEG, Tulsa, OK.
Yuan, S.Y. and Wang, S.X., 2011. A local f-x Cadzow method for noise reduction of seismic data obtained in complex formations. Petrol. Sci., 8: 269-277.
Yuan, Y.J., Zhou, Z.X., Niu, B.H., Wang, H.D., Liu, A.X., 2005. Briefly talk about processing techniques of improving the S/N ratio in seismic data processing. Oil Geophys. Prosp., 40: 168-171.
Zhou, Yu. and Garossino, P.G.A., 2005. High-energy noise attenuation of seismic data in the wavelet-transform domain. Integr. Comput.-Aid. Engineer., 12: 57-67.

APPENDIX A

ALGORITHM FOR THE S/N RATIO SPECTRUM OF DATA

In this Appendix, we review the algorithm for the signal to noise (S/N) ratio spectrum. The S/N ratio spectrum is estimated by

$$R_{SN} = \frac{P_s(f)}{P_N(f)}, \tag{A-1}$$

where $P_s(f)$ denotes the power spectrum of reflection signal, $P_N(f)$ denotes the power spectrum of noise, and R_{SN} denotes the S/N ratio spectrum.

We can get the power spectrum of reflection signal by

$$P_s(f) = \frac{1}{2(n-1)} \sum_{i=1}^{n-1} \left[A_i(f) \overline{A_{i+1}(f)} + A_{i+1}(f) \overline{A_i(f)} \right], \tag{A-2}$$

where n is the number of seismic traces and $A_i(f)$ is the amplitude spectrum of the *i-th* trace. The power spectrum of noise is written as follows:

$$P_N(f) = P_m(f) - P_s(f), \tag{A-3}$$

where $P_m(f)$ is the average amplitude spectrum, which can be obtained as follows

$$P_m(f) = \frac{1}{n}\sum_{i=1}^{n}\left[A_i(f)\overline{A_i(f)}\right]. \tag{A-4}$$